Selection of calibration particles for scanning surface inspection systems

George W. Mulholland, Nelson Bryner, and Walter Liggett

National Institute of Standards and Technology, Bldg. 224, Rm B360
Gaithersburg, MD 20899

Bradley W. Scheer

VLSI Standards, Incorporated, 3087 North First Street
San Jose, CA 95134-2006

Randal K. Goodall

International 300 mm Initiative, 2706 Montopolis Drive
Austin, TX 78741-6499

ABSTRACT

In response to the semiconductor industry's need for both smaller calibration particles and more accurately sized larger particles, a joint SEMATECH, National Institute of Standards and Technology, and VLSI Standards, Inc. project was initiated to accurately characterize 10 monodisperse polystyrene sphere suspensions covering the particle diameter range from 70 to 900 nm. The sizing analysis is being performed by electrical mobility analysis with a modified flow system to enable the measurement of the width of narrow size distributions. Results are presented on the mean size and the width of the distribution for candidate samples provided by five suppliers. The target sizes for the first set of particles are 72 nm, 87 nm, 125 nm, and 180 nm. Challenges for detecting "real world" particles are discussed including quantitative examples of the effects of refractive index, layered structure, and non-spherical shape on the light scattered by a particle.

Key words: differential mobility analyzer, electrical mobility, light scattering intensity, microcontamination, monodisperse spheres, polystyrene latex spheres, "real world" particles, wafer scanner, width of size distribution,

1. INTRODUCTION

The National Technology Roadmap for Semiconductors (NTRS) discusses particles as small as 60 nanometers (0.06μm) in diameter being a concern by year 2001. Polystyrene latex (PSL) spheres have been widely used by the wafer scanner manufacturers for calibrating their instuments. There are two limitations of existing PSL deposition standards. First, they are primarily limited to particle sizes of 100 nm and larger. Second, the calibration particles over the size range from 100 to 6000 nm have suffered in the past from being improperly sized, in some cases by as much as 25%[1]. VLSI Standards has observed the following inconsistencies between particle size and particle scattering: Company A's 135 nm "NIST-traceable " sphere scatters 42% less light intensity than company B's 136 nm sphere (1 nm difference, which should yield a scatter difference of only 4.5%); 173 nm spheres have 4% less scattered light intensity than 168 nm spheres even though the intensity should be 15% greater for the larger sphere. A project underway at the National Institute of Standards and Technology, partially funded by SEMATECH, has made great strides toward developing accurate monodisperse size standards covering the diameter range from 70 to 900 nm. In the first phase of this project, the following nominal sizes of polystyrene spheres have been targeted: 72 nm, 87 nm, 125 nm, and 180 nm. Several suppliers provided samples for each of these particle sizes. A differential mobility analyzer (DMA) and a scanning electron microscope (SEM) have been used at NIST to select the best sample for each targeted size in terms of mean particle size and width of the size distribution.

Of course, the "real world" particles that are a microcontamination issue in actual fabrication facilities are not PSL; they are silicon, silicon dioxide, aluminum, or a wide variety of other materials. These particles may be coated with an oxide layer, and they are not necessarily spherical. Before presenting the calibration study with PSL spheres, illustrative examples of the effects of refractive index and a surface layer on the core particle on the scattering intensity are presented. It is important to

0-8194-2250-9/96/$6.00

characterize the magnitude of these effects relative to PSL spheres to assess their significance on wafer scanner performance. These effects are computed based on Mie theory, which describes light scattering by an isolated sphere. A qualitative discussion of the effect of the surface on the scattering properties is included.

2. "REAL WORLD" PARTICLE EFFECTS

2.1 Light scattering theories

First we provide a brief review of some key results from light scattering theory. According to Rayleigh scattering theory, which is valid if particle size is small with respect to the wavelength, then the following equation for unpolarized light may be used to determine the scattered light intensity at a given angle Θ at a distance R:

$$I(\Theta) = \frac{I_0 \pi^4 D_p^6}{8 R^2 \lambda^4} \left| \frac{n^2 - 1}{n^2 + 2} \right|^2 (1 + \cos^2(\Theta)) \tag{1}$$

where I_o is the incident light intensity, D_p is the particle diameter, and n is the index of refraction of the particle [2].

The important relationship is that $I(\Theta)$ is proportional to D_p^6/λ^4, which is equivalent in this scattering regime to V_p^2/λ^4. In other words, the angular scattering intensity is proportional to the square of the particle *volume*, V_p. Effects of particle morphology are relatively unimportant. The dependence on refractive index is weaker than for particle size, but, as discussed below, it can still be a significant change going from a dielectric such as PSL to a conducting material such as aluminum.

The general solution for the scattered intensity for a spherical particle is known as the Mie solution. The scattered intensity for unpolarized incident light can be expressed as:

$$I(\Theta) = \frac{I_0 \lambda^2 (i_1 + i_2)}{8 \pi^2 R^2} \tag{2}$$

where i_1 and i_2 are the Mie intensity parameters for scattered light with s-polarization (polarization direction perpendicular to the plane defined by the incident and reflected beam)- and p-polarization (polarization direction parallel to this plane). The intensity parameters themselves are functions of refractive index, particle diameter, wavelength, and scattering angle. While the solution involves infinite series with Legendre polynomials and Bessel functions, there are a number of efficient algorithms for performing the sums for a wide range of sizes and refractive indices[3].

2.2 Effect of Refractive Index

When small particles are used for calibration, an accurate determination of index of refraction must be made for that particle to be useful. The importance of refractive index for small particles is clearly indicated by the Rayleigh theory expression in eq (1). Fortunately, the refractive index of polystyrene latex (PSL) spheres is well known[4]. Determination of the actual index of small PSL particles has been performed by levitating individual spheres and measuring the angle-resolved scattering produced by a beam incident on the particle. The actual index was back-calculated from this scattering signature[4]. Although this same methodology could be performed on other particle types, the procedure is extremely laborious and time-intensive, rendering it unusable on a production basis.

The total scattering intensity has been computed versus particle diameter for spherical particles with a wide range of refractive indices varying from PSL, a dielectric with $n=1.59$, to silver, a conductor with $n= 0.27+j4.18$, and aluminum with $n=1.3+j7.48$. The calculation is for the He-Ne laser wavelength, $\lambda=633$ nm. From Figure 1, it is seen that the effect of refractive index is relatively small, a factor of two or less, for particle diameters larger than about 1000 nm, but increases to a factor of 10 to 20 as the particle size decreases below 100 nm. This result is consistent with the Rayleigh prediction given by eq (1).

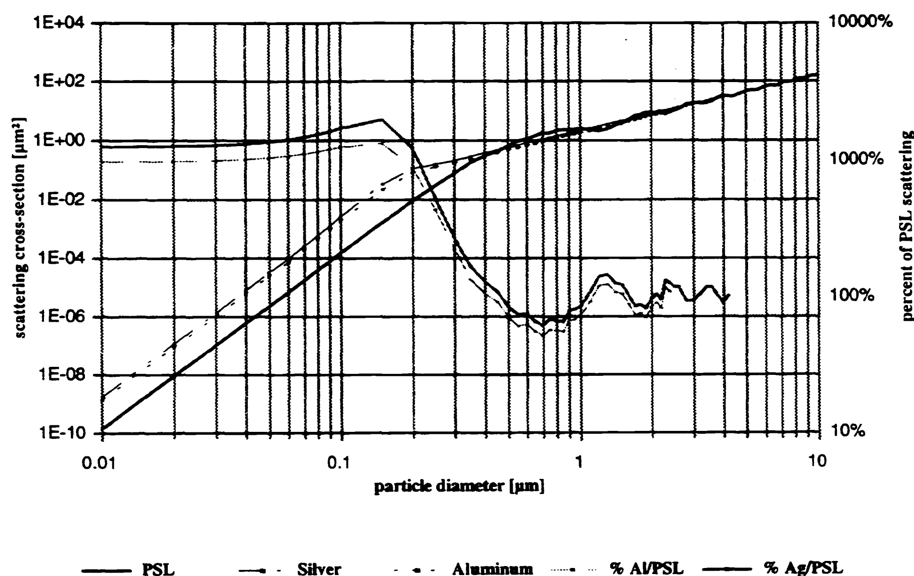

Figure 1. Calculated total integrated scatter from PSL, Ag, and Al spheres in free space. Note: effects of index are diminished as the sphere sizes become greater than the wavelength.

2.3 Layered Particles

The particles in many cases are expected to have a layered structure as a result of the formation of a surface oxide or from the condensation of a multicomponent vapor produced by plasma etching or chemical vapor deposition. In these cases it is not possible to make *a priori* assumptions about the index based on bulk properties alone. The surface area (πD_p^2) to volume ratio ($\pi D_p^3/6$) increases as the particle becomes smaller. Therefore, there must be an increasing awareness of any surface effects on the particle itself. This will take the form of a needed composite index (e.g., SiO_2 on Si, Al_2O_3 on Al, etc.).

Take for example a small silicon sphere. Since silicon will naturally produce a native oxide growth at room temperature known to be approximately 2 nm in thickness, this would imply that a particle of D_p = 14 nm would have a total volume of oxide which is nearly half of the particle volume. The refractive indices for SiO_2 and Si are n = 1.47 and n = 3.88+j0.02, respectively (at λ= 633nm). Therefore, the combined composite index is quite different and would lead to a total integrated scatter signal of roughly one-half the response of pure silicon alone[5]. Figure 2 shows the scattering relationship between Si and the same particle coated with SiO_2, emphasizing greater than twice the scatter from very small pure silicon particles. This distinction implies that caution must be used with the application and use of non-PSL particles in calibrating existing scanning surface inspection systems.

2.4 Non-Spherical Shape and Surface Effects

The analysis in the previous sections was limited to spherical particles. Many real world particles are non-spherical particles including agglomerate structures resulting from high temperature processes, faceted particles from ablation of crystalline structures, flakes and grainy particles from grinding, as well as others. For a large particle, the index is much less important. The critical factor is now the interplay of light with the particle morphology. Assuming a constant index, platelets will scatter less light than spheres which, in turn, will scatter less than cubes. In order to increase production yields, there must be a better fundamental understanding of the relationships between various particle types, morphologies, and the surfaces upon which they reside. A basic understanding of these theories can relate to practical problems of interpretation when particles are found on wafers, flat panel displays, or photomask surfaces.

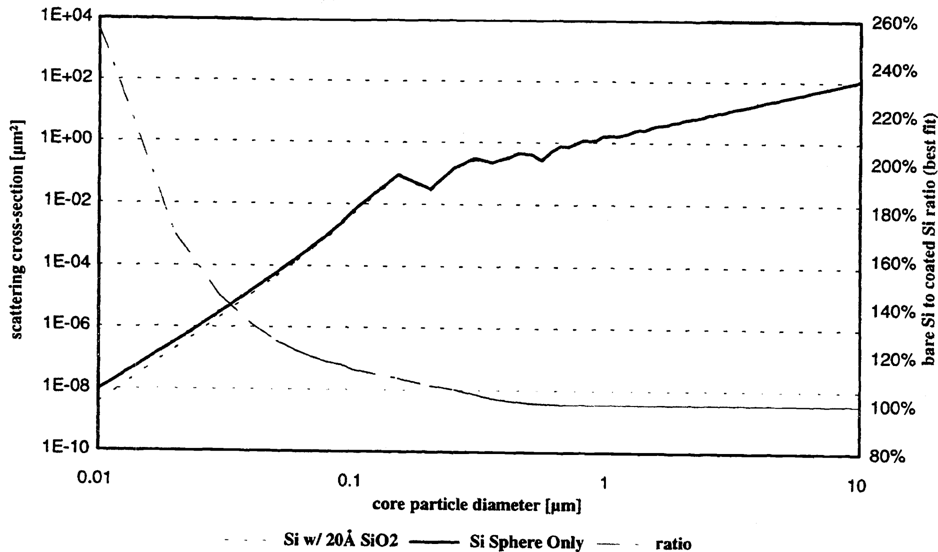

Figure 2. Calculated total integrated scatter from a pure silicon sphere (n=3.88+j0.23) versus silicon with a 2 nm coating of silicon dioxide (n=1.46, λ= 633nm). Note the reduced intensity for the coated particle.

Since there is a strong angular dependence of scattered light which varies as a function of particle size (with respect to the wavelength), it is not possible to make simple assumptions on how a given particle may react on a substrate without understanding the scattering phenomenon. Figures 3 and 4 indicate the calculated angular scatter for two particle sizes in free space. Scatter from particles on surfaces, or especially in the presence of films, is far more complicated.

To better understand the particle/substrate interaction, consider the example of the detector oriented to collect scattered light from the particle and surface interaction. The following two-component model provides a heuristic description of the scattering by a particle on the surface:

$$\delta C_{sc} = \delta C_b + R \cdot \delta C_f \quad . \tag{3}$$

This equation shows that the differential scattering cross-section for a particle on a surface, δC_{sc}, is a combination of the backscattered component of the radiation, δC_b, combined with the forward scattered component, δC_f, multiplied times the surface reflectivity, R. Here the term backscatter refers to light scattered directly from the particle, while forward scattered light refers to scattered light that is also reflected by the surface. The surface reflectivity itself is a function of wavelength, polarization, and angle of incidence. When combined with the complex scattering phenomenon, it becomes clear that this is a difficult problem to interpret, even when using a well characterized PSL sphere. However, recent experimental[6,7] and theoretical studies[8] are beginning to provide quantitative data and predictions for particles on a silicon surface.

3. PARTICLE SIZE CALIBRATION STANDARDS FOR WAFER SURFACE SCANNERS

As discussed above, there are limitations to the use of (PSL) polystyrene spheres as calibration standards for wafer scanners. Still PSL spheres are essential in the calibration process since they are available in monodisperse distributions ranging in size from 70 nm to more than 3,000 nm. Deposited on surfaces they provide essential calibration devices for wafer scanners. One limitation of the currently available spheres is the accuracy of the particle sizing. As discussed in the Introduction, results from existing calibration particles are inconsistent. This concern for accurate calibration particles prompted the SEMATECH Particle Counting and Microroughness Task Force to help sponsor a project to develop accurate calibration particles extending in particle diameter from 70 nm to 900 nm. The objectives of the project and the current status are discussed below.

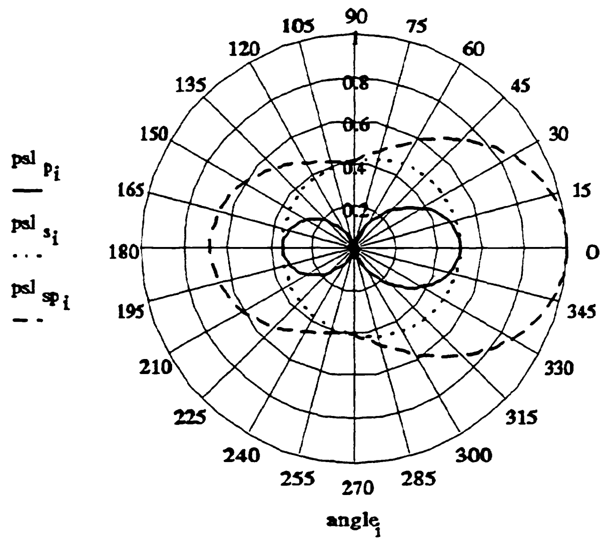

Figure 3. Angular dependence of scattered light from 100 nm PSL spheres (n=1.59, λ= 633nm). The subscripts s and p refer to the polarization state, whereas sp refers to the summation of both.

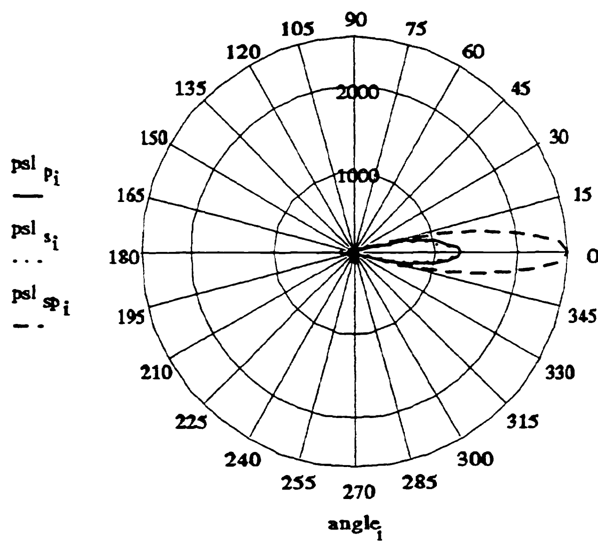

Figure 4. Angular dependence of scattered light from a 1.3 μm PSL sphere (n=1.59, λ = 633nm). Note the actual intensity units in figures 3 and 4 as well as the difference in the near forward scattering.

3.1 Specification for calibration particles

The major objective of this project is to make available to the semiconductor industry and, specifically, to the manufacturers of wafer scanners, accurate and monodisperse calibration particles. These particles would be provided in the form

of a suspension of spheres in high purity water (deionized and filtered) packaged in a vial holding several cm^3. The particle sizes are listed in Table 1. For particle sizes less than 200 nm, the light scattering intensity increases with the 6th power of particle diameter. This implies that a 20% increase in particle size will result in a tripling of the light scattering intensity. There is a wider gap between 87 and 125 nm, since the 100 nm particle size is available as a NIST Standard Reference Material (SRM 1963). For the larger particle sizes, the light scattering intensity approaches a 2nd power dependence on particle size. So in this case the 44% increase in particle size (square root of 2 spacing) corresponds to a factor of 2 increase in scattering intensity.

Table 1. Diameters for Calibration Particles

D_p, nm	First 4 Sizes	$D_{p,}$ nm
72	X	216
87	X	305
125	X	431
150		610
180	X	863

A list of specifications was developed for the desired calibration particles and then suppliers were asked to supply particles for consideration. The particle material was restricted to polystyrene. The first requirement of the particles is that the particle size be within 10% of the size listed in Table 1. The second requirement is that the standard deviation of the particle size distribution σ divided by the average particle diameter be less than or equal to 0.03 ($CV \leq 0.03$). Below the apparatus for making these measurements will be described and the results presented.

Other crucial requirements of the samples are that there be no biocide added to the suspension, that there be a minimum amount of surfactant, and there be minimum amount of contaminant in the water used to dilute the samples. This requirement is crucial since nonvolatile contaminants in the water would form a shell on the PSL spheres when the spheres are aerosolized or the contaminants themselves may cause additional peaks in the histogram. The other requirement is that there be no biological activity in the sample.

3.2 Experimental procedure

The particle measurement system consists of an aerosol generation system, a differential mobility analyzer (DMA) for size selection, and a condensation nucleus counter for monitoring the aerosol concentration (see Figure 5.). A brief description of the instrumentation and methodology is given below; a detailed description is given by Kinney *et al.*[9]. Several drops of the 1% by mass PSL spheres are diluted with 150 cm^3 de-ionized/filtered (0.2 μm pore size) water, mixed by shaking, and then placed in an ultrasonic bath to ensure uniform mixing. The suspension is nebulized (107 Kpa at gauge, 15 psig) to form an aerosol with droplets containing the PSL spheres. The water evaporates as the aerosol flows at 83 cm^3/s (5 L/min) through a diffusion drier and is mixed with 40 cm^3/s (2.4 L/min) of clean, dry air. The PSL sphere aerosol is charged with a bipolar charger and then flows through the DMA.

The DMA consists of an inner cylinder rod connected to a variable (0 to -11,000 V) DC power supply and an outer annular tube connected to ground. Clean sheath air flows through the axial region while the charged aerosol enters through an axisymmetric opening along the outer cylinder. The positively charged PSL spheres move radially towards the center rod under the influence of the electric field. Near the bottom of the classifying region, a fraction of the air flow consisting of near-monodisperse (single sized) aerosol is extracted through a slit in the center rod. The particles next flow to a condensation nucleus counter, where the number concentration is measured. A typical measurement sequence is to measure the number concentration as a function of the applied voltage.

The quantity measured by the DMA is the electrical mobility, Z_p, defined as the velocity a particle attains under a unit electric field. Knutson and Whitby[10] derived an expression for the average value of Z_p for the particles entering the slit

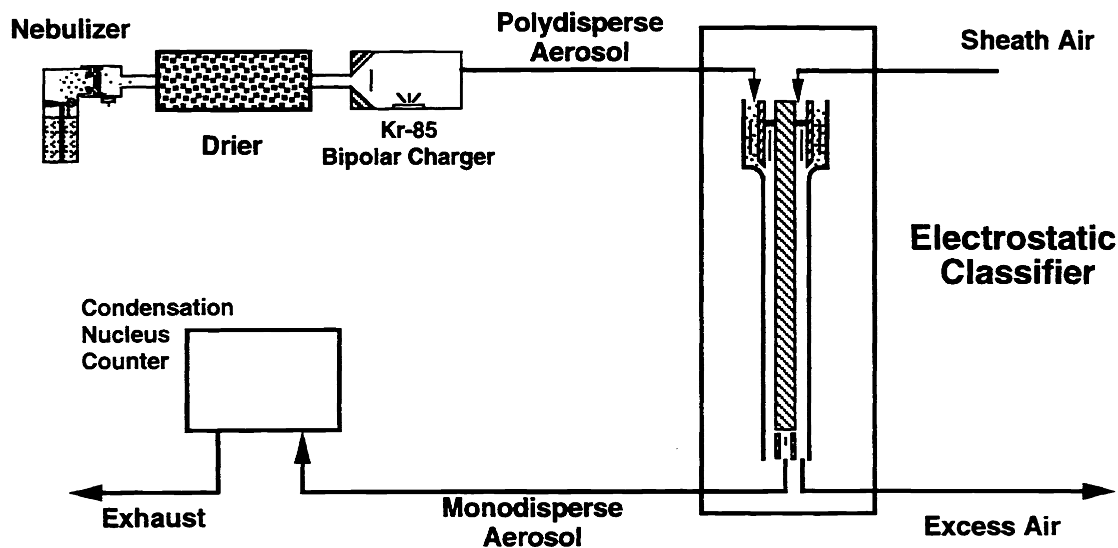

Figure 5. The particle measuring system includes an aerosol generation system (nebulizer), the differential mobility analyzer, and the condensation nucleus counter.

involving the electrode voltage, V, the sheath air flow rate, Q_c, the inner and outer radii of the cylinders, r_1 and r_2, and the length of the central electrode down to the slit, L.

$$Z_p = \frac{Q_c}{2\pi VL}\ln(r_2/r_1) \quad . \tag{4}$$

This equation is valid provided the sheath air flow, Q_c is equal to the excess flow, Q_m, leaving the classifier. They obtained the following expression for the range in the electrical mobility, ΔZ_p, involving the inlet aerosol flow, Q_a.

$$\Delta Z_p = \frac{Q_a}{4\pi VL}\ln(r_2/r_1) \quad . \tag{5}$$

The ratio $\Delta Z_p/Z_p$ provides a measure of the resolution limit of the measurement given by

$$\frac{\Delta Z_p}{Z_p} = \frac{2Q_a}{Q_c} \quad . \tag{6}$$

A major focus of this study was the measurement of the widths of the size distributions of the particles provided by the various suppliers.

An expression for the electric mobility of a singly charged particle involving the particle diameter is obtained[10] by equating the electric field force with the Stokes Drag force,

$$Z_p = \frac{\epsilon C(D_p)}{3\pi\mu D_p} \quad , \tag{7}$$

where μ is the air viscosity and ϵ is the electron charge. The Cunningham slip correction $C(D_p)$, which corrects for the non-

continuum behavior for particle sizes smaller than the mean free path of air, is given by

$$C(D_p) = 1 + K_n[A_1 + A_2\exp(-a_3/K_n)] \quad , \tag{8}$$

where K_n is the Knudsen Number. For a measured value of Z_p, the particle diameter, D_p, is obtained iteratively from eqs (7) and (8).

As mentioned above the major challenge of this study was to measure the widths of the size distributions of the polystyrene spheres supplied by various suppliers. As indicated by eq(6), the smaller the ratio Q_a/Q_c, the higher the resolution of the classifier. In this study we operated the DMA with a flow ratio of 0.025 with a sheath air flow, Q_c, of 333 cm^3/s (20 L/min), and the aerosol inlet flow, Q_a, at a flow of 8.3 cm^3/s (0.5 L/min). In addition to having a small flow ratio for high resolution, it is also imperative that the sheath air and excess air flows, Q_c and Q_m, be equal. Otherwise the resolution will be broadened. The resolution of the flow meters is on the order of $\pm 1\%$ leading to a flow difference on the order of 5 cm^3/s for the larger flows. Since the total inlet and exit flows are equal, the resulting percentage difference in the aerosol flow could be 50%. To overcome this difficulty the excess air was recirculated back into the sheath air assuring, in principle, that the flows were matched. Through trial and error a system evolved with the following key features illustrated in Figure 6: two small pumps and buffer tanks before and after the pumps to minimize pulsation, cooling water and an ambient heat exchanger to cool the recirculated air, a filter to remove the particles, silica gel to remove water vapor, and a thermometer to monitor the temperature. The measured leak rate was less than 0.017 cm^3/s or less than 0.5% of the aerosol flow.

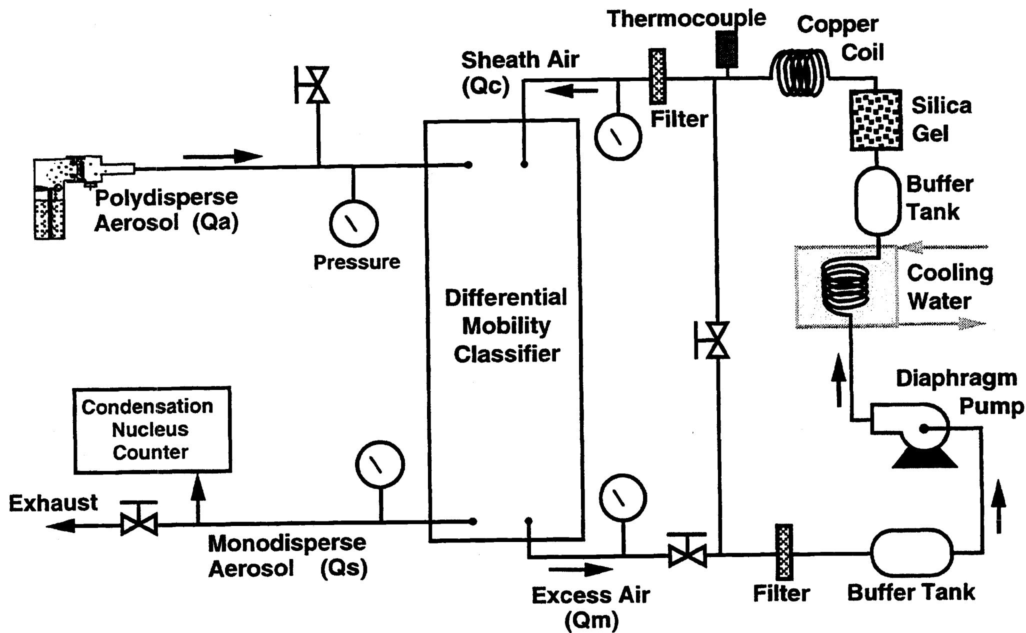

Figure 6. The excess air is recirculated to match the sheath flow in this closed loop operation of the DMA.

A typical experiment consists of starting the nebulizer, setting the voltage, collecting number concentration data for 45 seconds, then repeating the same process for typically a total of five increasing voltages. Then the same sequence would be repeated but decreasing the voltage. From a preliminary experiment, the voltage for the peak number concentration would be determined along with the voltage increments corresponding to number concentrations of about 2/3 of the peak and 1/3 of the peak. The peak voltage in the case shown in Figure 7 is 2300 V, and the incremental increase is 150 V. While it is not readily apparent from the Figure 7, for each voltage setting the concentration reading is steady within $\pm 10\%$ for 20 seconds and these

points are used in computing the average number concentration for each voltage setting. The signals from the three flowmeters (Q_a, Q_c, and Q_m), the electrode voltage, and the number concentration are recorded via a computer.

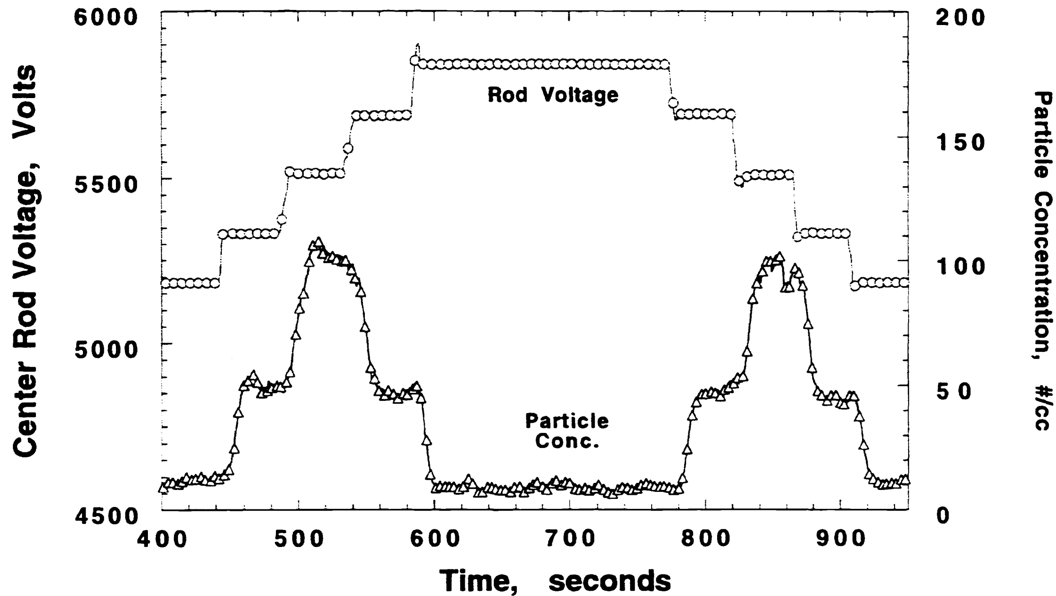

Figure 7. The center rod voltage and particle concentration are plotted for a typical sequence of voltage steps used to determine the particle size distribution.

3.3 Size distribution analysis

For each voltage setting the corresponding electrical mobility, Z_p, is obtained from eq (4). The particle diameter, in turn, is obtained from eqs (7) and (8) iteratively by estimating the value of D_p, computing the resulting Cunningham slip correction from eq (8), and then computing the value of D_p from eq (7). This computed value is then used as a new guess and the process repeated until the values of D_p converge. In Figure 8 a representative size distribution is plotted in terms of the measured number concentration normalized by the maximum reading.

The two key parameters determined from the size distribution are the diameter, D_m, corresponding to the maximum in a fit of the data points, and the half-width of the distribution at half-height, HWHH. The first three points and the last three points are fitted with cubic polynomials with the requirement that the 0th, 1st, and 2nd derivatives be continuous at the middle point where the two polynomials meet. A computer program was developed to determine both D_m and HWHH. Figure. 8 illustrates the method for one size distribution. In a few cases this method did not work, and a straight line was drawn between the 1st and 2nd points or the fourth and fifth points.

3.4 Results

Table 2 provides a listing of all the samples provided by the suppliers. Each supplier, A-E, provided samples with their measured size within about 10% of the specified size listed in Table 2.

Figure 9 contains the results of three repeat measurements of the size distribution to illustrate the repeatability of the measurement method. The values of D_m for all three measurements are in a very narrow range from 164.9 nm to 165.1 nm, which corresponds to about 0.1% of the mean value. The variation in HWHH is 0.3 nm, which is similar in magnitude to the variation in D_m, 0.2 nm; however, because the values of HWHH are so small, the percent change, 10%, is much greater than for D_m.

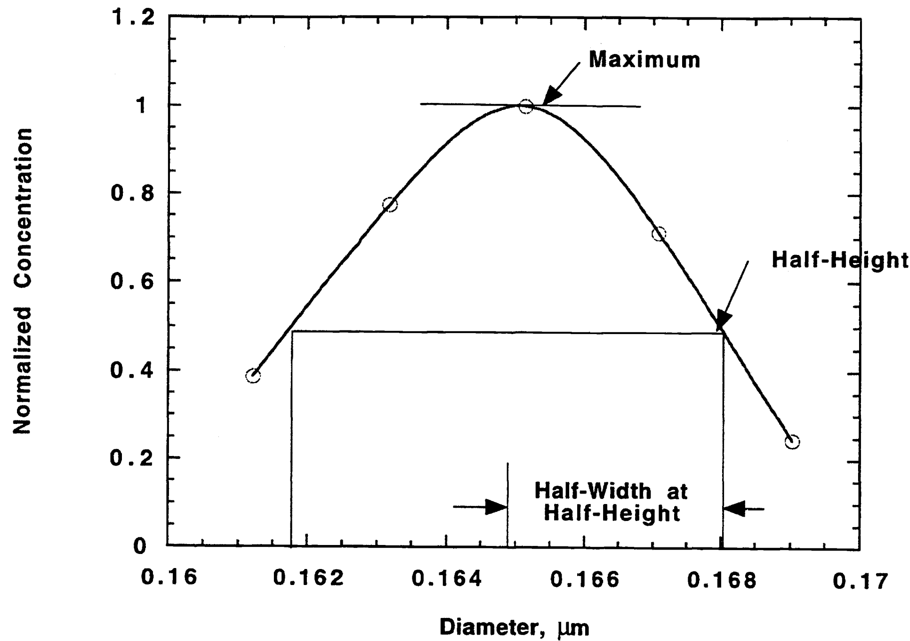

Figure 8. The half-width at half-height is determined from cubic spline fits with the first and second derivative matched at the peak data point.

Table 2. Polystyrene Sphere Samples Characterized at NIST

D_p, μm	A	B	C	D	E
0.072	X	X	X	X	
0.087		X	X	X	X
0.125		X	X	X	X
0.180	X	X	X	X	X
0.216	X	X	X	X	X
0.305	X	X	X	X	X

Figure 10 shows that most of the size measurements by the suppliers differ by more than 5% from the size measurements performed by the DMA. To assess the accuracy of the classifier itself, the 100.7 nm NIST SRM 1963 was measured with the classifier, and the size was 2.4% larger than the certified size. The other sizes measured by the classifier are also overestimated by about this same amount. The fact that difference between the suppliers' measured sizes and the DMA result are as large as 20%s demonstrates that accuracy of the size measurement is an issue for particle sizes less than 300 nm.

Figure 11 indicates that most of the measured sizes exceed the diameters specified in Table 1 with half of the samples exceeding the target particle size by at least 5%. As discussed below, the final particles selected are systematically larger than the original target sizes by about 5%.

The second major focus of this study was the screening of particles based on the width of the size distribution. The repeatability of the HWHH measurements are on the order of 5% to 10% of the mean value. The effect of the finite resolution of the DMA has not been taken into account in the analysis of the HWHH so the measured values are than the true values of the HHHW of the particles. The DMA provides a relative measure of the widths of the size distribution. Figure 12 shows the

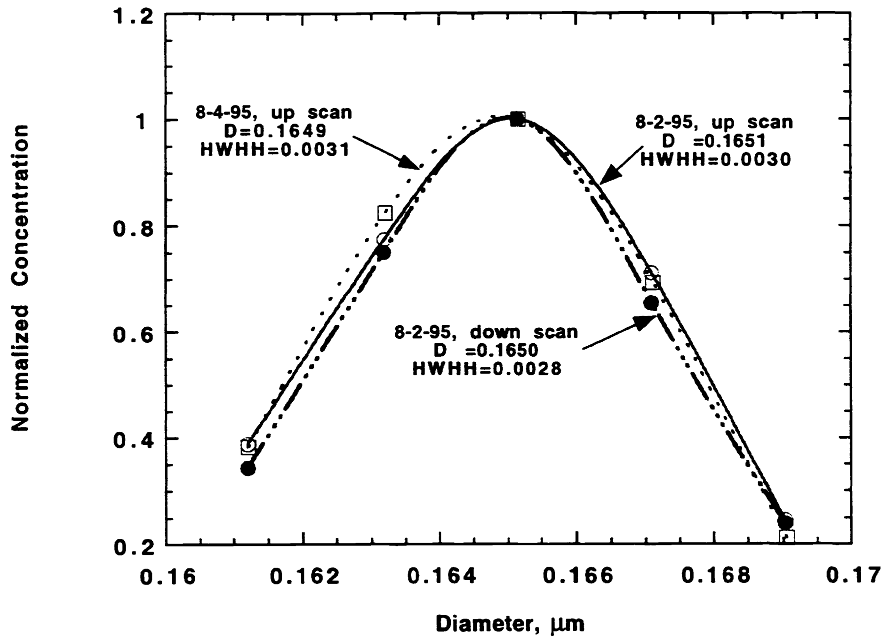

Figure 9. The size distribution is plotted based on upward voltage scan followed by a downward voltage scan and then a repeat upward scan two days later.

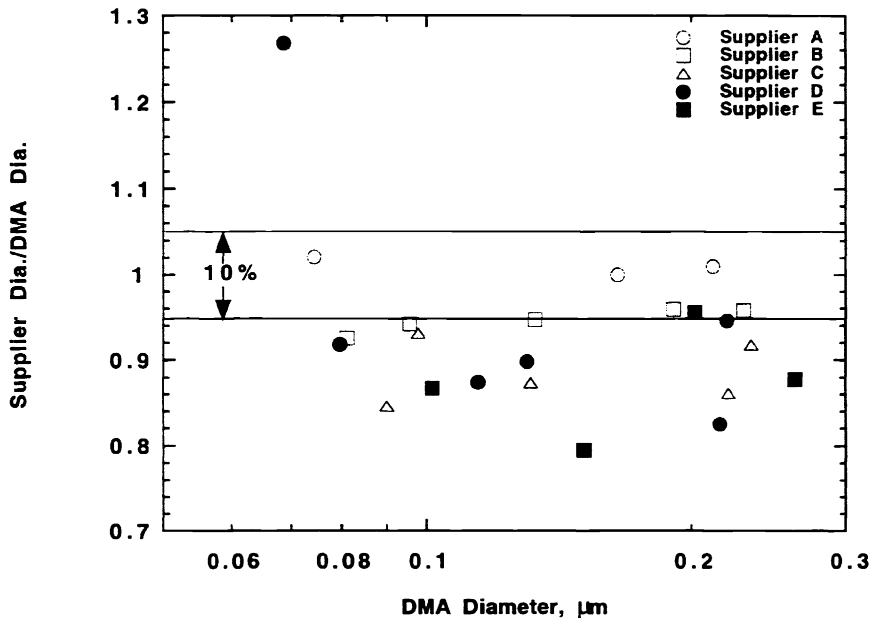

Figure 10. The mean particle size determined by the supplier is compared with the size determined by the DMA in this study.

size distribution of four different samples with a target diameter of 87 nm. The HWHH/D_m for the various size distributions vary from a minimum of 0.046 to a maximum of 0.084. In two cases, supplier C#1 and supplier E, a relatively high concentration of small particles is observed. It is clear from this figure that the DMA is a useful instrument for screening samples based

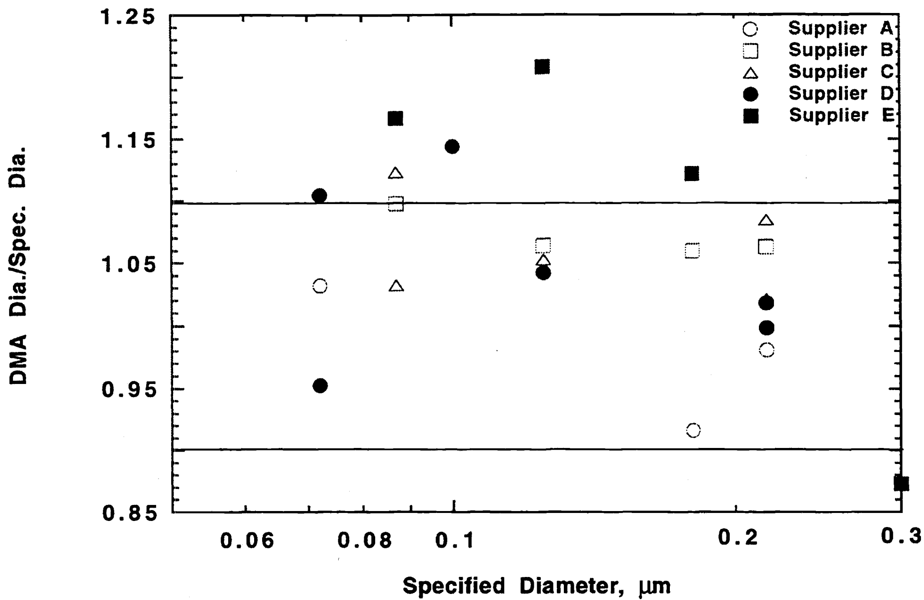

Figure 11. The mean particle size measured by the DMA is compared with the particle sizes specified in Table 1.

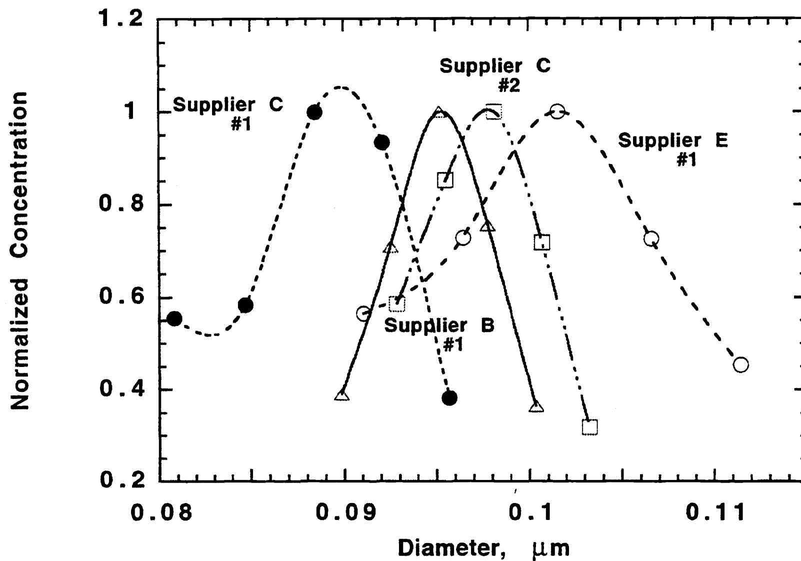

Figure 12. Comparison of size distribution of nominal 87 nm spheres supplied by three suppliers.

on the width of the size distribution. In this case the final choice becomes a compromise, since supplier C #1 is closest in size, but supplier B has the narrowest size distribution. The discussion of the final selection will be given in the next section.

In Figure 13 we have included the specified size and HWHH for each sample and indicated the target range for particle diameter and HWHH as a box. The best choice is the one closest to the specified size with the smallest value of HWHH (closest to the diameter axis). For the two smallest sizes it is seen that none of the samples satisfy the HWHH criterion; for the larger three there are several that meet the HWHH criterion. There is a continuing challenge to develop smaller size particles with a monodisperse size distribution.

In addition to size distribution analysis, for selected samples electron microscopy was performed. These selected samples are identified below. The DMA measurements focussed on the center of the size distribution. Scanning electron microscopy was used to determine the number of off-size large particles with diameters in excess of twice the value of D_m and off-size small particles with diameters less than half the value of D_m. The number of particles viewed is typically on the order of 400 - 600. For five of the six samples the percentage of off-size small or large particles was less than 0.4%. For sample #1,B - 180 nm, the values were much larger with the undersized making up 2% and the oversized making up almost 4% of the particles analyzed.

3.5 Recommended samples

The recommendations for the best samples by the SEMATECH Particle Counting and Microroughness Task Force selected for each target particle size is shown in Table 3. It was found that most of the sizes measured with the DMA were larger than the ideal size, however, it was found that a number of good candidate particles were available for sizes about 5% larger than the ideal sizes. It was realized that the uniform spacing of the particle diameters was more important than closeness to the target size; that is, the crucial issue is that all the particle sizes be consistently high or low relative to the specified size. The amended selection criteria are the width of the size distribution and the uniformity in the spacing of D_m, the peak size. For the smallest two sizes, the width of the distribution was the key factor because of lack of narrow distributions. For the larger three, both choices easily satisfied the width requirements; so in this case the deciding feature was the uniformity in the particle spacing with each size 3% to 5% larger than the ideal size. Another important practical advantage is that the number of suppliers is minimized with four of the 5 highest ranked samples available from a single supplier.

3.6 Future Work

Work is in progress to accurately measure four of these five particle sizes both at NIST and at VLSI Standards, Inc. The plan is to complete the measurements and uncertainty analysis by October, 1996. These calibrated particles would then be available for distribution. Selection of the other 5 particle sizes listed on Table 1 is anticipated to begin in the Fall, 1996.

Table 3. Recommended Sizes

Rank, Supplier	Ideal Size, μm	DMA Size[a], μm	hwhh/peak	DMA/Ideal
1, D	0.072	0.078	0.041	1.08
2, A	0.072	0.073	0.057	1.01
1, B	0.087	0.093	0.046	1.07
2, C	0.087	0.095	0.056	1.09
1, B	0.125	0.130	0.019	1.04
2, D	0.125	0.127	0.015	1.02
1, B	0.180	0.186	0.018	1.03
2, E	0.180	0.197	0.016	1.09
1, B	0.216	0.224	0.018	1.04
2, D	0.216	0.215	0.015	1.00

[a] DMA sizes corrected by multiplicative factor of 0.977 based on apparent size measurement of the 0.1007 μm SRM.

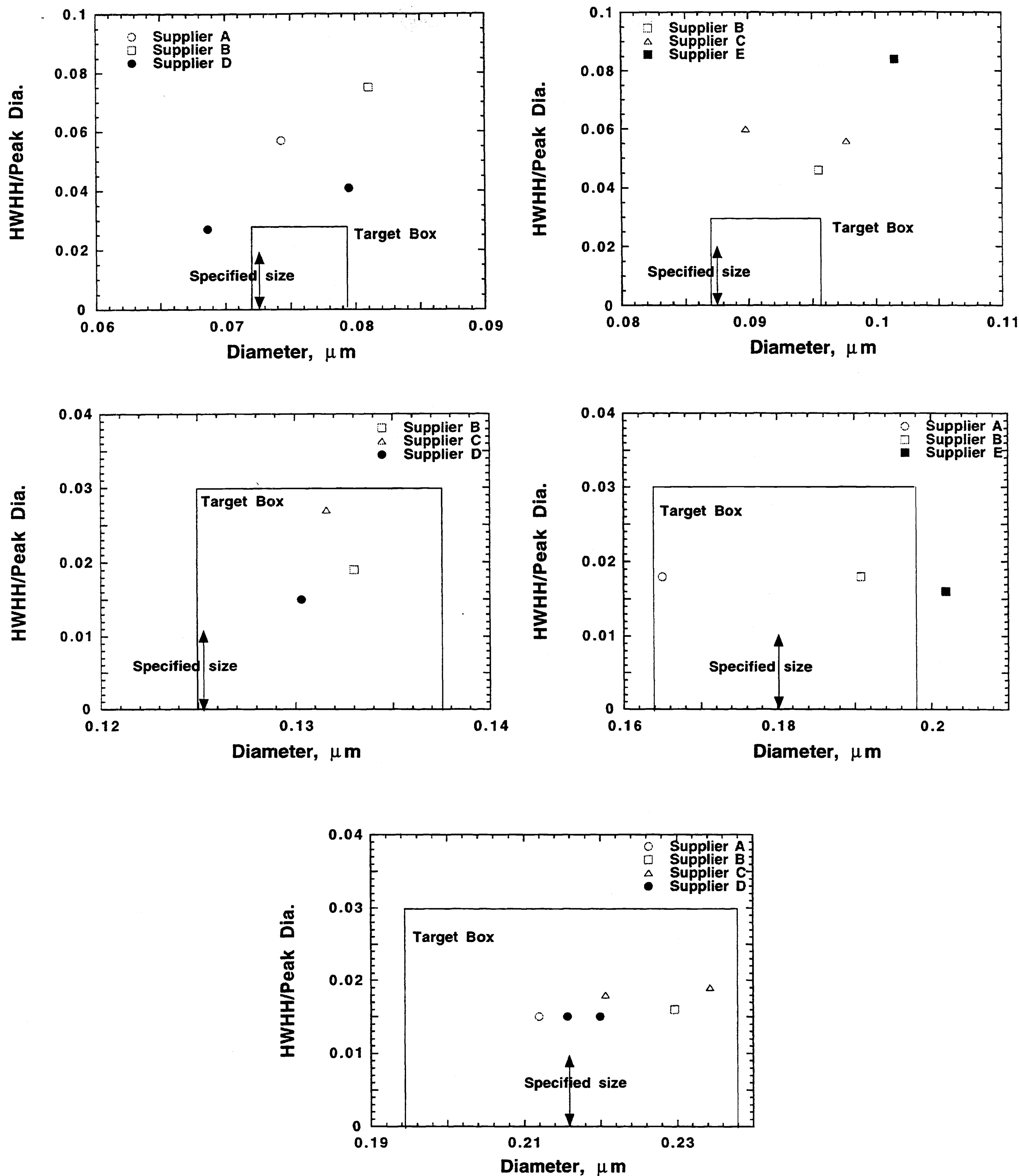

Figure 13. Measured D_m and half-width at half-height relative to the target range.

Acknowledgement

The authors recognize the technical and financial contributions by the SEMATECH Particle Counting and Microroughness Task Force to this study.

References

1. Hinds, W.C., *Aerosol Technology, Properties, Behavior, and Measurement of Airborne Particles*, p. 385, John Wiley and Sons, New Y York, 1982.

2. van de Hulst, H.C., *Light Scattering by Small Particles*, Dover Publications, New York, 1981.

3. Bohren, C.F. and Huffman, D.R., *Absorption and Scattering of Light by Small Particles*, Wiley Interscience, New York, 1983.

4. Mulholland, G.W. and Marx, E., "Size and Refractive Index Determination of Single Polystyrene Spheres," *Journal of Research of the National Bureau of Standards*, Vol. 88, No. 5, pp. 321-338, 1983.

5. Scheer, B.W., "Reference Wafers for Haze and Particle Instruments Evaluation," *Proceedings of the Particles, Haze, and Microroughness on Silicon Wafers Symposium*, San Jose, CA, Sept. 1994.

6. Huff, H.R., Goodall, R.K., Williams, E., Woo, K.S., Liu, B.Y.H., Warner, T., Hirleman, E.D., Gildersleeve, K., Bullis, W.M., Scheer, B.W., "Measurement of Silicon Particles by Laser Surface Scanning and Angle-resolved Light Scattering," *Proceedings of Microcontamination 1994 Conference*, San Jose, CA, 1994.

7. Stover, J.C., Bernt, M.L., Church, E.C., and Takacs, "Measurement and Analysis of Scatter from Silicon Wafers", *Proc. Spie*, Vol. 2260, p.21, 1994.

8. Eremin, Y., "Simulation of Light Scattering by a Particle on a Wafer Surface," submitted to *Applied Optics*.

9. Kinney, P.D., Pui, D.Y.H., Mulholland, G.W., and Bryner, N.P., "Use of the Electrostatic Classification Method to Size 0.1 μm SRM Particles - A Feasibility Study", *J. Res. Natl. Inst. Stand. Technol*, Vol. 96, pp. 147-176, 1991.

10. Knutson, E.O. and Whitby, K.T., "Aerosol Classification by Electric Mobility: Apparatus, Theory, and Applications", *J. Aer. Sci.*, Vol. 6, pp. 443-451, 1975.